

2.3. Effect of MgNPs-Fe₃O₄ on Cell Viability, Cell Membrane Damage, and Apoptosis

Treatment with MgNPs-Fe₃O₄ for 24 h did not affect cell viability as assessed by the Alamar Blue assay. However, treatment with 100 µg/mL MgNPs-Fe₃O₄ for 72 h caused a significant reduction in cell viability (Figure 3). Significant LDH leakage was detected following treatment with 100 µg/mL MgNPs-Fe₃O₄; lower concentrations had no effect (Figure 4). As shown in Figure 5a, treatment with 100 µg/mL MgNPs-Fe₃O₄ for 24 h caused a small but significant increase in the percentage Annexin V-staining cells; however, these values were greatly below that caused by H₂O₂ (Figure 5b).

Figure 3. Effect of Fe₃O₄ magnetic nanoparticles (MgNPs-Fe₃O₄) on viability of A549 cells. A549 cells were treated with 0 (control), 1, 10 or 100 µg/mL MgNPs-Fe₃O₄ for 24 or 72 h. Cell viability was assessed using the Alamar Blue assay. Data are presented as the mean ± SD of 3 independent experiments. * *p* < 0.05 vs. control.

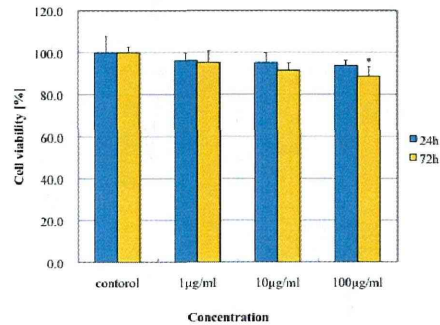


Figure 4. Effect of MgNPs-Fe₃O₄ on lactate dehydrogenase (LDH) release by A549 cells. A549 cells were treated with 0 (control), 1, 10 or 100 µg/mL MgNPs-Fe₃O₄ for 24 h. LDH release was assessed by formazan absorbance (LDH Cytotoxicity Assay Kit). Data are presented as the mean ± SD of 3 independent experiments. ** *p* < 0.01 vs. control.

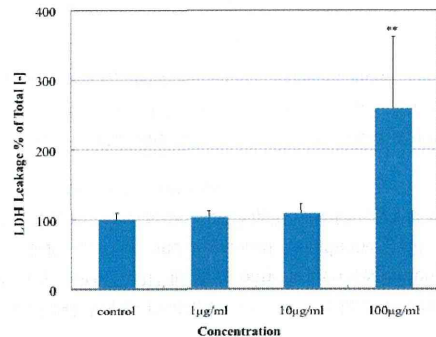
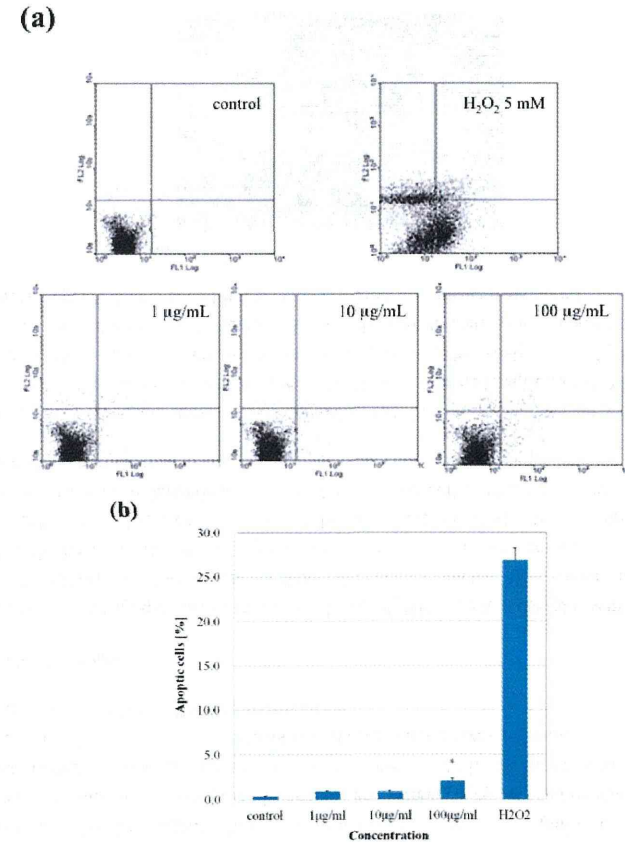


Figure 5. Effect of Fe₃O₄ magnetic nanoparticles (MgNPs-Fe₃O₄) on apoptosis in A549 cells. A549 cells were treated with 0 (control), 1, 10 or 100 µg/mL MgNPs-Fe₃O₄ for 24 h; cells were treated with 5 mM H₂O₂ for 24 h as a positive control. Apoptosis of A549 cells treated with MgNPs-Fe₃O₄ or H₂O₂ was determined by flow cytometry based on propidium iodide/Annexin V staining patterns; (a) Representative flow cytometry of one set of triplicate experiments; (b) Percentages of apoptotic cells from flow cytometry analysis. Apoptotic cells include early apoptotic cells (AnnexinV+/PI-) and late apoptotic or necrotic cells (AnnexinV+/PI+). Data are presented as the mean ± SD of three independent experiments. * *p* < 0.05 vs. control.



2.4. Effect of MgNPs-Fe₃O₄ on ROS Production, Intracellular Glutathione, and 8-OH-dG Levels in DNA

As shown in Figure 6, MgNPs-Fe₃O₄ caused a dose-dependent increase in ROS production with concentrations of 10 and 100 µg/mL. Figure 7 demonstrates that MgNPs-Fe₃O₄ caused a dose-dependent decrease in the GSH level; GSH was reduced by 65% with 100 µg/mL MgNPs-Fe₃O₄. The 8-OH-dG levels were increased approximately 8- and 14-fold above control with 10 and 100 µg/mL MgNPs-Fe₃O₄, respectively (Figure 8). ROS production by MgNPs-Fe₃O₄ is well known to be involved in the cytotoxic response in various cell types. Fe₃O₄, a mixture of FeO and Fe₂O₃, is unstable and can readily undergo oxidation to yield γ -Fe₂O₃ + Fe²⁺ [7,9,16]. The free Fe²⁺ ions can react with hydrogen peroxide and oxygen produced by the mitochondria to produce highly reactive hydroxyl radicals and Fe³⁺ ions [17] that can damage DNA, proteins, polysaccharides, and lipids *in vivo*. Similar to our findings, previous studies have shown that Fe₃O₄ elicited an increase in oxidative DNA lesions in A549 cells with minimal effect on cell viability [7–9]. Of the non-enzymatic antioxidants, GSH represents the major intracellular redox buffer in all cell types. Abundant in all cell compartments, it constitutes the first line of the cellular defense mechanism against oxidative injury [16]. Previous studies demonstrated that ROS generation following GSH depletion caused mitochondrial damage and up-regulation of pro-apoptosis mediators [2,7,18]. We found MgNPs also significantly reduced the GSH level. However, our data suggest that the shift in balance toward pro-oxidant mechanisms exerts little impact on cell viability.

Figure 6. Effect of MgNPs-Fe₃O₄ on production of reactive oxygen species (ROS) by A549 cells. A549 cells were treated with doses 0 (control), 1, 10 or 100 µg/mL MgNPs-Fe₃O₄ for 24 h. ROS production was determined using the CM-H₂DCFDA assay. Data are presented as the mean ± SD of three independent experiments. ** $p < 0.01$ vs. control.

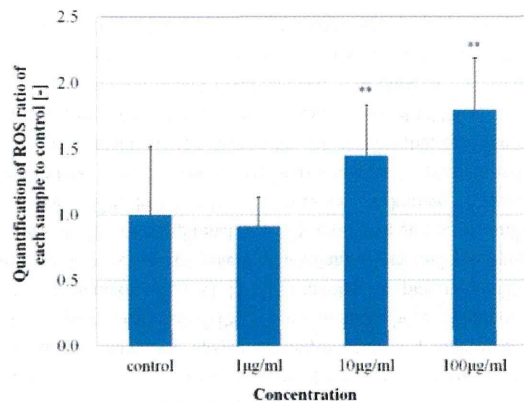


Figure 7. Effect of MgNPs-Fe₃O₄ on intracellular glutathione (GSH) levels in A549 cells. A549 cells were treated with 0 (control), 1, 10 or 100 µg/mL MgNPs-Fe₃O₄ for 24 h. GSH levels were assessed by luciferin bioluminescence (GSH-Glo Glutathione Assay Kit). Data are presented as the mean ± SD of three independent experiments. Significantly different from the untreated control at ** $p < 0.01$ vs. control.

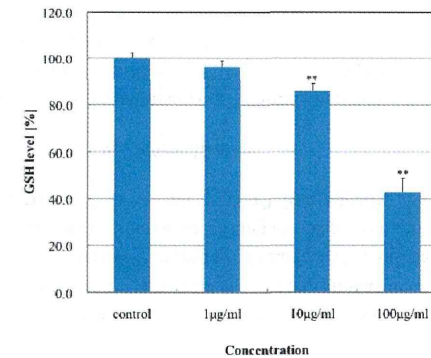
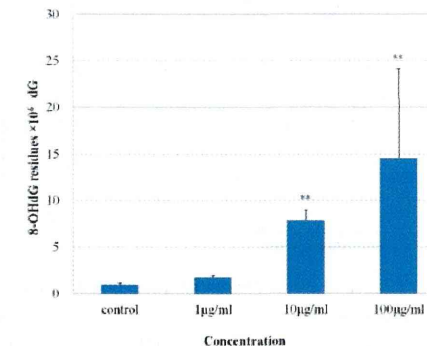


Figure 8. Effect of MgNPs-Fe₃O₄ on 8-hydroxy-deoxyguanosine (8-OH-dG) levels in A549 cells. A549 cells were treated with 0 (control), 1, 10 or 100 µg/mL MgNPs-Fe₃O₄ for 72 h. DNA was extracted by the sodium iodide method; 8-OH-dG levels were determined using HPLC-ECD. Data are presented as the mean ± SD of three independent experiments. * Significantly different from the untreated control at ** $p < 0.01$ vs. control.

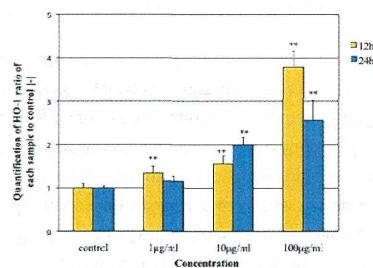


2.5. Expression of the Heme Oxygenase-1 (HO-1) Gene

As shown in Figure 9, the transcript level of the *HO-1* was induced in a dose-dependent manner after 12 and 24 h of MgNPs-Fe₃O₄ exposure, however its transcription level at 100 mg/mL exposure after 24 h was reduced compared to after 12 h. Oxidative stress is caused by an imbalance in the level

of ROS and a biological system's ability to detoxify the reactive intermediates [16]. Cells possess both enzymatic and non-enzymatic mechanisms to counterbalance the cytotoxicity and genotoxicity caused by ROS [16]. In the lungs, the major enzymatic antioxidants are superoxide dismutases (SODs), catalase, and glutathione peroxidase (GSH-Px); others include those examined in this study, HO-1, thioredoxin (TR), and glutaredoxin (GLRX). HO-1 is involved in playing a major role in degradation of heme to biliverdin, but has recognized potent anti-inflammatory and anti-apoptotic effects [17,19]. HO-1 is induced mainly at the transcriptional level by oxidative stress, pro-inflammatory mediators, and some growth factors [18]. HO-1 mRNA expression is known to mediate antioxidant and cytoprotective effects and has been considered useful as a marker for particle-induced oxidative stress. Park *et al.* [20] showed that treatment of a human bronchial epithelial cell line with TiO₂-MgNPs for four hours caused dose-dependent increases in mRNA expression of HOG-1, glutathione-S-transferase, and catalase; mRNA expression level of HO-1 had returned to baseline by 24 h [20]. Napierska *et al.* [21] also showed a marked induction of HO-1 mRNA in the endothelial cell at six hours after treatment of SiO₂-NPs, but reduction of HO-1 mRNA at 24 h. Our results appear to be same as these two studies.

Figure 9. Effect of MgNPs-Fe₃O₄ on mRNA expression of the *HO-1* gene in A549 cells. The expression level of the *HO-1* was normalized according to the expression level of β -actin. Data are presented as the mean \pm SD of three independent experiments. ** $p < 0.01$ vs. control.

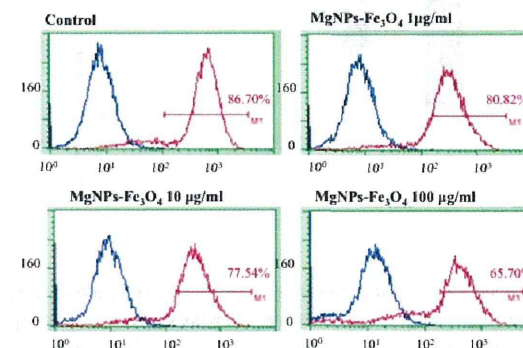


2.6. Effect of MgNPs-Fe₃O₄ on CD44⁺ Cell Fraction in A549 Cells

MgNPs-Fe₃O₄ caused a dose-dependent reduction in the CD44⁺ subpopulation (Figure 10). CD44 is a cell surface glycoprotein that mediates cellular adhesion to the extracellular matrix and is involved in multiple processes, including inflammation, cell migration, signaling, and tumor metastasis [13,22]. CD44 is up-regulated in the damaged epithelium of asthma patients, and is believed to be involved in tissue repair by localizing chemokines and growth factors to the disrupted epithelium [23]. CD44 is also a marker of certain cancer stem cells [24], in which it functions to defend cancer cells against oxidative stress by increasing GSH synthesis [25]. CD44 has also been reported to be involved in the protective effect of hyaluronate on constitutive DNA damage by ROS in A549 cells [26]. Consistent with the previously noted reduction in GSH and increase in 8-OH-dG levels, we found that MgNPs-Fe₃O₄ markedly decreased the CD44⁺ cell fraction of A549 cells. Thus, these results highlight another mechanism by which MgNPs-Fe₃O₄ impair redox control and damage DNA in A549 cells. Our

results also offer the possibility that CD44 may be a marker MgNP-Fe₃O₄-induced cytotoxicity; however, further study is warranted.

Figure 10. Effect of Fe₃O₄ magnetic nanoparticles (MgNPs-Fe₃O₄) on CD44⁺ cell fraction in A549 cells. A549 cells were treated with 0 (control), 1, 10 or 100 µg/mL MgNPs-Fe₃O₄ for 24 h. Cells were labeled with mouse anti-human CD44 monoclonal antibody; level of CD44⁺ cells was determined by flow cytometry.



3. Experimental Section

3.1. MgNPs-Fe₃O₄

MgNPs-Fe₃O₄ were obtained from the Toda Kogyo Corporation (Otake, Hiroshima, Japan). As specified by the manufacturer, MgNPs in powder were spherical, with an average particle size of 10 nm, as measured by transmission electron microscopy (TEM), and a surface area of 100–120 m²/g. In suspension, the particle size ranged from 60 to 100 nm as measured by dynamic light scattering (DLS) and zeta potential ranged from –30 to –40 mV at pH 10. Bare MgNPs-Fe₃O₄ were used in this study.

3.2. Preparation of MgNPs-Fe₃O₄ in Culture Medium

MgNPs-Fe₃O₄ were sterilized by ultraviolet (UV) irradiation and suspended in phosphate-buffered saline (PBS), Ham's F-12 alone, and Ham's F-12 medium containing 10% fetal bovine serum (FBS) and 100 U/mL penicillin-streptomycin to yield a concentration of 1, 10 or 100 µg/mL. Suspensions were sonicated at 30 W for 10 min using an Ultrasonic Homogenizer VP-050 (TAITAE, Koshigaya, Saitama, Japan).

3.3. Cell Line

A549 human lung epithelial cells were purchased from American Tissue Type Culture Collection (Manassas, VA, USA). Cells were incubated in Ham's F-12 Medium with 10% fetal bovine serum

(FBS) and 100 U/mL penicillin–streptomycin in 5% CO₂ at 37 °C. Cells were maintained at a density of 60%–70% confluence in 100 mm dishes, and used in log-phase of growth.

3.4. Characterization of MgNP-Fe₃O₄ Suspensions in Cell Culture Medium

The average hydrodynamic size and size distribution of MgNPs-Fe₃O₄ in cell culture media and their intracellular localization were determined by DLS using a Fiber-Optics Particle Analyzer FPAR-1000 (Otsuka Electronics, Hirakata, Osaka, Japan). MgNPs-Fe₃O₄ were suspended in Ham's F-12 Medium with or without 10% FBS and supplements, or in phosphate-buffered saline (PBS).

3.5. Cellular Uptake of MgNPs-Fe₃O₄ in A549 Cells

The cellular uptake of MgNPs-Fe₃O₄ in A549 cells was analyzed as follows.

3.5.1. Transmission Electron Microscopy (TEM)

A549 cells were fixed with 3% glutaraldehyde in 0.1 M cacodylate buffer (pH 7.3) at 4 °C for 4 h. Samples were post-fixed with 2% osmium tetroxide at 4 °C for 2 h, dehydrated, and embedded in epoxy resin. Ultrathin sections (80 nm) were then stained with uranyl acetate and lead citrate, and observed by TEM.

3.5.2. Flow Cytometry Assay

A549 cells were treated with 0, 1, 10 or 100 µg/mL MgNPs-Fe₃O₄ for 24 h, and then trypsinized and suspended in medium. Cellular uptake of MgNPs-Fe₃O₄ was analyzed using flow cytometry (Millipore, Billerica, MA, USA), in which the intensities of forward-scattered (FS) and side-scattered (SS) light are proportional to cell size and intracellular density of MgNPs-Fe₃O₄, respectively. A total of 30,000 cells were measured per sample.

3.6. AlamarBlue Assay

Cell viability was determined using the alamarBlue assay (Alamar Biosciences, Sacramento, California, USA) according to the manufacturer's instructions. Briefly, cells (1.0 × 10⁴ cells/well) were incubated with MgNPs-Fe₃O₄ (0, 1, 10 or 100 µg/mL) for 72 h at 37 °C. AlamarBlue (10%) was added to each well and incubated for 200 min. Metabolically active cells reduced the dye to a fluorescent form, which was measured using a plate reader (excitation/emission: 570 nm/600 nm; Viento XS, DS Pharma Biomedical, Suita, Osaka, Japan). Cell viability was determined by linear interpolation of the emission from cells treated with 0.1% saponin (0% viability) and untreated cells (100% viability).

3.7. Lactate Dehydrogenase (LDH) Release Assay

LDH release assay to assess membrane integrity was performed using LDH-cytotoxicity assay kit (BioVision, CA, USA) according to the manufacturer's instructions. Cells cultured in 24-well plates (1.5 × 10⁴ cells/well) were treated with 0, 1, 10 or 100 µg/mL MgNPs-Fe₃O₄ for 24 h at 37 °C. Plates were then centrifuged at 250×g for 5 min. The supernatant of each well was transferred to a fresh, flat

bottom 96-well culture plate containing 100 µL reaction mixture, and incubated for 30 min at room temperature. Formazan absorbance—an index of the number of lysed cells—was measured by a microplate reader at 500 nm (Viento XS, DS Pharma Biomedical, Osaka, Japan).

3.8. Apoptosis by Flow Cytometry (FCM)

A549 cells (1.0 × 10⁶ cells) were cultured on 100-mm culture dishes, and treated with 0, 1, 10 or 100 µg/mL MgNPs-Fe₃O₄ for 24 h at 37 °C. Cells were harvested, washed gently with PBS, collected by centrifugation, and then stained using an Annexin V-FITC Kit (Beckman Coulter, Marseille, France) following the manufacturer's instructions. Cells were stained with Annexin V and propidium iodide (PI, Sigma-Aldrich, St. Louis, MO, USA), and analyzed by flow cytometry (Becton Dickinson, Franklin Lakes, NJ, USA) within 1 h of staining using the FL1 (FITC) and FL3 (PI) lines.

3.9. Measurement of Intracellular Reactive Oxygen Species (ROS)

ROS were measured using the CM-H₂DCFDA assay (Invitrogen, Carlsbad, CA, USA) according to the manufacturer's instructions. Cells (1.0 × 10⁴ cells/well) in 24 well-plates were treated with 0, 1, 10 or 100 µg/mL MgNPs-Fe₃O₄ for 24 h at 37 °C. A fresh stock solution of 5 mM CM-H₂DCFDA was prepared in DMSO and diluted to a final concentration of 1 µM in PBS. Cells were washed with PBS, followed by incubation with 50 µL of working solution of the fluorochrome marker CM-H₂ DCFDA for 30 min. Fluorescent images were obtained using an IX2N-FL-1 microscope (Olympus, Tokyo, Japan), and analyzed using imaging soft (Photoshop Elements 8, Adobe systems, Tokyo, Japan). The data were expressed as percentage of the unexposed control.

3.10. Intracellular Reduced Glutathione (GSH) Assay

Intracellular GSH level was determined using a GSH-Glo Glutathione assay kit (Promega, Madison, WI, USA) according to the manufacturer's instructions. Briefly, cells were seeded in 96-well plates and treated with 0, 1, 10 or 100 µg/mL MgNPs-Fe₃O₄ for 24 h at 37 °C. The cells were washed with DPBS, and the GSH-Glo reagent was added to each well for 30 min at room temperature to allow the cells to convert a luciferin derivative into luciferin. Reconstituted luciferin detection reagent was then added to each well for 15 min, and the luminescent signal was measured with a Glomax multi detection system (Promega, Madison, WI, USA).

3.11. Analysis of 8-Hydroxy-2'-Deoxyguanosine (8-OH-dG) in DNA

A549 cells were incubated with 0, 1, 10 or 100 µg/mL MgNPs-Fe₃O₄ for 72 h at 37 °C (5% CO₂). The nuclear DNA was isolated by the sodium iodide method. The 8-OH-dG levels were analyzed by HPLC-ECD methods as previously described [27]. The amount of 8-OH-dG in the DNA was determined by comparison to authentic standards, and expressed as the number of 8-OH-dG per 10⁶ deoxyguanosine (dG) residues.

3.12. Oxidative Stress-Related Gene Expression Analysis

A549 cells were treated with 0, 1, 10, or 100 µg/mL MgNPs-Fe₃O₄ for 24 h at 37 °C. Total RNA was isolated using ISOGEN (Nippon Gene, Tokyo, Japan), and cDNA was produced using a mixture containing Superscript RNase H Reverse Transcriptase (Invitrogen, Carlsbad, CA, USA), oligo dT primer, and 2.5 mmol/L dNTP. Quantitative real-time PCR was conducted using the LINE GENE real-time PCR detection system (BioFlux, Tokyo, Japan) with the SYBR Premix Ex Taq Perfect Real Time Kit (Takara Bio. Inc., Otsu, Japan). The PCR reaction consisted of initial thermal activation at 95 °C for 10 s and 40 cycles. Each cycle was as follows: 95 °C for 5 s; 60 °C for 26 s. PCR products were verified by analysis of heat-dissociation curves and amplification plots. Quantitative values were acquired from linear regression of the PCR standard curve. The primer sequences of the amplified genes are as follows [28,29]; *Heme oxygenase-1*, forward 5'-GGTGATAGAAGAGCCAAGAC-3' and reverse 5'-GCAGAATCTTGCACCTTGTG-3', *β-actin*, forward 5'-GGATGCAGAAGGAGATCACTG-3' and reverse 5'-CGATCCACACGGAGTACTTG-3'.

3.13. Immunostaining and Flow Cytometric Analysis for CD44⁺ Cell Fraction

A549 cells were treated with 0, 1, 10 or 100 µg/mL MgNPs-Fe₃O₄ for 24 h at 37 °C. Cells were then labeled in a PBS solution with a mouse anti-human CD44 monoclonal antibody conjugated with fluorescein isothiocyanate (clone SFF-2, Millipore, Billerica, MA, USA) for 1 h at room temperature. A mouse IgG immunoglobulin and dye conjugate IgG was used as control for non-specific binding. Flow cytometric analysis was performed with a Guava-EasyCyte*HT using Guava Express Pro software (Millipore, Billerica, MA, USA) gating for CD44⁺ cells. A minimum of 10,000 cells was measured per sample.

3.14. Statistical Analysis

Data are presented as the mean ± standard deviation (SD). Differences between treated and untreated control cells were determined using one-way ANOVA followed by Dunnett's test. Differences were considered statistically significant at $p < 0.05$.

4. Conclusions

MgNPs-Fe₃O₄ up to a concentration of 100 µg/mL exerted minimal effect on viability of A549 cells, despite causing a significant reduction in antioxidant capacity and an increase in oxidative damage to DNA. Increased expression of an oxidative stress-related gene was not sufficient to prevent the decrease in GSH content. The decrease in the CD44⁺ cell fraction was consistent with the observed drop in GSH concentration and increase in 8-OH-dG level.

Acknowledgments

This research was supported in part by a Grant-in-Aid for the Global COE Program from the Ministry of Education, Culture, Sports, Science and Technology of Japan, a Grant-in-Aid for Research

on Risk of Chemical Substances from the Ministry of Health, Labour and Welfare of Japan, and a Research Grand-in-Aid from Magnetic Health Science Foundation.

Conflict of Interest

The authors report no conflict of interest. The authors are responsible for the content and writing of the paper.

References

- Chakraborty, M.; Jain, S.; Rani, V. Nanotechnology: Emerging tool for diagnostics and therapeutics. *Appl. Biochem. Biotechnol.* **2011**, *165*, 1178–1187.
- Ramesh, V.; Ravichandran, P.; Copeland, C.L.; Gopikrishnan, R.; Biradar, S.; Goornavar, V.; Ramesh, G.T.; Hall, J.C. Magnetite induces oxidative stress and apoptosis in lung epithelial cells. *Mol. Cell. Biochem.* **2012**, *363*, 225–234.
- Parveen, S.; Misra, R.; Sahoo, S.K. Nanoparticles: A boon to drug delivery, therapeutics, diagnostics and imaging. *Nanomedicine* **2012**, *8*, 147–166.
- Hilger, I.; Kaiser, W.A. Iron oxide-based nanostructures for MRI and magnetic hyperthermia. *Nanomedicine* **2012**, *7*, 1443–1459.
- Chen, B.; Sun, Q.; Wang, X.; Gao, F.; Dai, Y.; Yin, Y.; Ding, J.; Gao, C.; Cheng, J.; Li, J.; *et al.* Reversal in multidrug resistance by magnetic nanoparticle of Fe₃O₄ loaded with adriamycin and tetrandrine in K562/A02 leukemic cells. *Int. J. Nanomed.* **2008**, *3*, 277–286.
- Sato, A.; Itcho, N.; Ishiguro, H.; Okamoto, D.; Kawai, K.; Kasai, H.; Kurioka, D.; Uemura, H.; Kubota, Y.; Watanabe, M. Magnetic nanoparticles of Fe₃O₄ enhance docetaxel-induced prostate cancer cell death. *Int. J. Nanomed.* **2013**, in press.
- Singh, N.; Jenkins, G.J.; Asadi, R.; Doak, S.H. Potential toxicity of superparamagnetic iron oxide nanoparticles (SPION). *Nano Rev.* **2010**, *1*, 5358.
- Karlsson, H.L.; Cronholm, P.; Gustafsson, J.; Möller, L. Copper oxide nanoparticles are highly toxic: A comparison between metal oxide nanoparticles and carbon nanotubes. *Chem. Res. Toxicol.* **2008**, *21*, 1726–1732.
- Kim, J.E.; Shin, J.Y.; Cho, M.H. Magnetic nanoparticles: An update of application for drug delivery and possible toxic effects. *Arch. Toxicol.* **2012**, *86*, 685–700.
- Lewinski, N.; Colvin, V.; Drezek, R. Cytotoxicity of nanoparticles. *Small* **2008**, *4*, 26–49.
- Klein, S.; Sommer, A.; Distel, L.V.; Neuhuber, W.; Krysch, C. Superparamagnetic iron oxide nanoparticles as radiosensitizer via enhanced reactive oxygen species formation. *Biochem. Biophys. Res. Commun.* **2012**, *425*, 393–397.
- Holgate, S.T. Epithelial damage and response. *Clin. Exp. Allergy.* **2000**, *1*, 37–41.
- Kitamura, H.; Okudela, K.; Yazawa, T.; Sato, H.; Shimoyamada, H. Cancer stem cell: Implications in cancer biology and therapy with special reference to lung cancer. *Lung Cancer* **2009**, *66*, 275–281.
- Hong, S.C.; Lee, J.H.; Kim, H.Y.; Park, J.Y.; Cho, J.; Lee, J.; Han, D.W. Subtle cytotoxicity and genotoxicity differences in superparamagnetic iron oxide nanoparticles coated with various functional groups. *Int. J. Nanomed.* **2011**, *6*, 3219–3231.

15. Wiogo, H.T.R.; Lim, M.; Bulmus, V.; Yun, J.; Amal, R. Stabilization of magnetic iron oxide nanoparticles in biological media by fetal bovine serum (FBS). *Langmuir* **2011**, *27*, 843–850.
16. Birben, E.; Sahiner, U.M.; Sackesen, C.; Erzurum, S.; Kalayci, O. Oxidative stress and antioxidant defense. *World Allergy Organ J.* **2012**, *5*, 9–19.
17. Tulis, D.A.; Durante, W.; Liu, X.; Evans, A.; Peyton, K.J.; Schafer, A.I. Adenovirus-mediated heme oxygenase-1 gene delivery inhibits injury-induced vascular neointima formation. *Circulation* **2001**, *104*, 2710–2715.
18. Morita, T. Heme oxygenase and atherosclerosis. *Thromb. Vasc. Biol.* **2005**, *25*, 1786–1795.
19. Durante, W. Heme oxygenase-1 in growth control and its clinical application to vascular disease. *J. Cell Physiol.* **2003**, *195*, 373–382.
20. Park, E.J.; Yi, J.; Chung, K.H.; Ryu, D.Y.; Choi, J.; Park, K. Oxidative stress and apoptosis induced by titanium dioxide nanoparticles in cultured BEAS-2B cells. *Toxicol. Lett.* **2008**, *180*, 222–229.
21. Napierska, D.; Rabolli, V.; Thomassen, L.C.J.; Dinsdale, D.; Princen, C.; Gonzalez, L.; Poels, K.L.C.; Kirsch-Volders, M.; Lison, D.; Martens, J.A.; *et al.* Oxidative stress induced by pure and iron-doped amorphous silica nanoparticles in subtoxic conditions. *Chem. Res. Toxicol.* **2012**, *25*, 828–837.
22. Yasuda, M.; Nakano, K.; Yasumoto, K.; Tanaka, Y. CD44: Functional relevance to inflammation and malignancy. *Histol. Histopathol.* **2002**, *17*, 945–950.
23. Leir, S.H.; Baker, J.E.; Holgate, S.T.; Lackie, P.M. Increased CD44 expression in human bronchial epithelial repair after damage or plating at low cell densities. *Am. J. Physiol. Lung Cell Mol. Physiol.* **2000**, *278*, L1129–L1137.
24. Leung, E.L.; Fiscus, R.R.; Tung, J.W.; Tin, V.P.; Cheng, L.C.; Sihoe, A.D.; Fink, L.M.; Ma, Y.; Wong, M.P. Non-small cell lung cancer cells expressing CD44 are enriched for stem cell-like properties. *PLoS One* **2010**, *5*, e14062.
25. Nagano, O.; Okazaki, S.; Saya, H. Redox regulation in stem-like cancer cells by CD44 variant isoforms. *Oncogene* **2013**, in press.
26. Zhao, H.; Tanaka, T.; Mitalitski, V.; Heeter, J.; Balazs, E.A.; Darzynkiewicz, Z. Protective effect of hyaluronate on oxidative DNA damage in WI-38 and A549 cells. *Int. J. Oncol.* **2008**, *32*, 1159–1167.
27. Kawai, K.; Li, Y.S.; Kasai, H. Accurate measurement of 8-OH-dG and 8-OH-Gua in mouse DNA, urine and serum: Effects of X-ray irradiation. *Genes Environ.* **2007**, *29*, 107–114.
28. Miyake, M.; Fujimoto, K.; Anai, S.; Ohnishi, S.; Kuwada, M.; Nakai, Y.; Inoue, T.; Matsumura, Y.; Tomioka, A.; Ikeda, T.; *et al.* Heme oxygenase-1 promotes angiogenesis in urothelial carcinoma of the urinary bladder. *Oncol. Rep.* **2011**, *25*, 653–660.
29. Wang, C.; Tian, Y.; Lei, B.; Xiao, X.; Ye, Z.; Li, F.; Kijlstra, A.; Yang, P. Decreased IL-27 expression in association with an increased Th17 response in Vogt-Koyanagi-Harada disease. *Invest. Ophthalmol. Vis. Sci.* **2012**, *53*, 4668–4675.

© 2013 by the authors; licensee MDPI, Basel, Switzerland. This article is an open access article distributed under the terms and conditions of the Creative Commons Attribution license (<http://creativecommons.org/licenses/by/3.0/>).

Transfection efficiency influenced by aggregation of DNA/polyethylenimine max/magnetic nanoparticle complexes

Satoshi Ota · Yoshiyuki Takahashi · Asahi Tomitaka · Tsutomu Yamada · Daisuke Kami · Masatoshi Watanabe · Yasushi Takemura

Received: 11 December 2012 / Accepted: 12 April 2013 / Published online: 25 April 2013
© Springer Science+Business Media Dordrecht 2013

Abstract Gene delivery using magnetic nanoparticles (MNPs) is known as magnetofection and is an efficient non-viral gene delivery system. γ -Fe₂O₃ nanoparticles (primary diameter = 29 nm) and Fe₃O₄ nanoparticles (primary diameter = 20–30 nm) coated with deacylated linear polyethylenimine (PEI max) were prepared and conjugated with DNA. The dependency of transfection efficiency on the weight of MNPs, viability of HeLa cells, and size of DNA/PEI max/MNP complexes was evaluated. Transfection efficiency initially increased with the weight of the complexes; however, it decreased with further increase in weight. In contrast, cell viability increased with further increase in weight. Cytotoxicity assay showed that the decline in transfection efficiency at higher weights was not attributable to cytotoxicity of DNA/PEI max/MNP complexes. The DNA/PEI max/MNP complexes aggregated because of DNA binding and pH interaction with the medium. Aggregation

depending on the weight of MNPs was confirmed. The number of complexes was estimated from the size distribution. In addition, the dependency of the transfection efficiency on aggregation was assessed with respect to cellular endocytic pathways using the complexes. The complexes were internalized through clathrin-dependent endocytosis, which was a size-dependent pathway. This study reveals that decreased transfection efficiency was associated with the extent of aggregation, which was induced by high weight of MNPs.

Keywords Magnetofection · Magnetic nanoparticles · Aggregation · Cytotoxicity · Endocytosis

Introduction

Recently, magnetic nanoparticles (MNPs) have attracted considerable attention as transfection vectors. Non-viral transfection vectors such as cationic polymers and cationic liposomes are more biocompatible than viral vectors; however, their transfection efficiency is lower (De Smedt *et al.* 2000; Guo *et al.* 2007). MNPs guide DNA into the target tissue and transfect targeted cells rapidly, and the application of magnetic fields leads to the translocation of MNPs inside the cells (Scherer *et al.* 2002). Coupling non-viral transfection vectors with iron oxide nanoparticles

S. Ota (✉) · Y. Takahashi · T. Yamada · M. Watanabe · Y. Takemura
Faculty of Engineering, Yokohama National University,
Yokohama 240-8501, Japan
e-mail: ota-satoshi-gw@ynu.ac.jp

A. Tomitaka
Department of Materials Science and Engineering,
University of Washington, Seattle, WA 98195, USA

D. Kami
Department of Cardiac Supports, Kyoto Prefectural
University of Medicine, Kyoto 602-8566, Japan

such as polyethylenimine (PEI) (Scherer et al. 2002), polyamidoamine dendrimer (Pan et al. 2007), and PEI/poly(ethylene glycol)/chitosan copolymer (Kievit et al. 2009)-coated iron oxide nanoparticles facilitate high transfection efficiency and biocompatibility. Furthermore, surface-modified silica (Roy et al. 2005) and gold (Ghosh et al. 2008) nanoparticles have been used instead of iron oxide nanoparticles for gene delivery vectors.

PEI has a cationic charge owing to protonation of the amino nitrogen under physiological conditions (Boussif et al. 1995). PEI conjugates with DNA through electrostatic forces because PEI is cationic and DNA is anionic (Kircheis et al. 2001; Oku et al. 2001). PEI is known as both a coating and a transfection reagent (Boussif et al. 1995; Seino et al. 2009). First, MNPs tend to aggregate because of van der Waals interactions, whereas coating with PEI prevents aggregation via electrostatic repulsion (Seino et al. 2009). Second, DNA/PEI/MNP complexes are guided to cell surfaces by cationic-anionic interactions between PEI and the cell membrane (Payne et al. 2007). Third, the complexes are internalized into the cells by endocytosis promoted by ligand/receptor interactions between PEI and cell surface receptors (Godbey et al. 1999; Scherer et al. 2002). During endocytosis, the complexes are engulfed by cell membrane invaginations and encapsulated into membrane-bound vesicles known as endosomes (Sahay et al. 2010). PEI elicits proton sponge effects characterized by proton accumulation followed by passive chloride influx into endosomes. This influx causes osmotic swelling leading to endosome disruption thereby protecting DNA contained in the complexes from lysosomal degradation (Kichler et al. 2001; Akincl et al. 2005). PEI takes two forms: linear and branched. Linear PEI is less toxic compared with branched PEI (Jeong et al. 2001). In this study, PEI max, which is a deacylated linear PEI, was coated on MNPs. These MNPs were used as transfection vectors. Linear PEI contains residual *N*-acyl groups that hinder gene transfection (Thomas et al. 2005). Deacylation of linear PEI promotes transfection.

With respect to magnetofection, transfection efficiency is determined primarily by magnetic force on the particles, particle configuration in the medium, and endocytic pathway, depending on the size of particles. Magnetic force depends on magnetization, volume,

magnetic permeability of MNPs (Pankfurst et al. 2003; Furlani and Xue 2012), and magnetic field gradient (Pankfurst et al. 2003; Akiyama et al. 2010; Furlani and Xue 2012). Configuration of nanoparticles in the medium is influenced by pH, concentration of particles, surface-coating agents, and serum protein (Steitz et al. 2007; Wang et al. 2009; Wigo et al. 2012). The influences of nanoparticle size on endocytosis have been investigated with poly (D, L-lactide-co-glycolide) nanoparticles fractionated to small- (<100 nm) and large-size (>100 nm) nanoparticles (Prabha et al. 2002), gold nanoparticles of size 45, 70, and 110 nm (Wang et al. 2010), and latex fluorescent beads of defined size (50–1000 nm) (Rejman et al. 2004). These studies show that high rate of cellular internalization is achieved with smaller-sized nanoparticles.

The dependency of transfection efficiency on the weight of MNPs was evaluated by determining the cytotoxicity and size of DNA/PEI max/MNPs complexes in HeLa cells. The effect of the size of the complexes on endocytic pathways was also assessed to confirm the influence of size on transfection efficiency. The novelty of this study lies in the confirmation of the MNP weight response of transfection efficiency in terms of cytotoxicity, aggregation of complexes, and endocytic pathway. Moreover, relationships between transfection efficiency and aggregation are confirmed for both γ -Fe₂O₃ and Fe₃O₄ nanoparticles.

Materials and methods

Materials and surface coating

γ -Fe₂O₃ nanoparticles (primary diameter = 29 nm) and Fe₃O₄ nanoparticles (primary diameter = 20–30 nm) were purchased from CIK NanoTek and Nanostructured & Amorphous Materials, Inc. These nanoparticles were coated with PEI max (mw 40,000) purchased from Nacalai Tesque and Polysciences, Inc.

γ -Fe₂O₃ nanoparticles (200 mg) were dispersed in 10 ml solution of 1.0 mg/ml PEI max by supersonication for 10 min. This solution was purified by centrifugation at 743×g ($R = 7.39$ cm) for 15 min. The supernatant was centrifuged at 10,000×g ($R = 8.8$ cm) for 30 min. The precipitate was collected as PEI max-coated γ -Fe₂O₃ nanoparticles (Kami et al. 2011a). For Fe₃O₄ nanoparticles,

200 mg of nanoparticles were dispersed in 40 ml solution of 1.0 mg/ml PEI max. The rest of the process was the same as for γ -Fe₂O₃ nanoparticles.

Transfection and preparation of MNP of different densities

HeLa cells from a human cervical carcinoma line were cultured in Dulbecco's modified Eagle medium (DMEM) supplemented with 10 % fetal bovine serum (FBS) and 1 % penicillin–streptomycin (PS). The cells were seeded in 35 mm dishes at a density of 200,000 cells/well on the day prior to transfection. The cells were incubated at 37 °C in a humidified atmosphere containing 5 % CO₂.

To evaluate the dependency of transfection efficiency on the weight of MNPs, solutions of 1 mg/ml PEI max and various densities of PEI max-coated MNPs were prepared. PEI max and PEI max-coated MNPs solutions (7.5 μ l) were mixed with 2.5 μ g of plasmid DNA expressing enhanced green fluorescent protein (EGFP) in sterile water for 15 min. DNA/PEI max complexes and DNA/PEI max/MNP complexes were added to 1 ml medium. Each medium containing DNA/PEI max complexes or DNA/PEI max/MNP complexes was added to the cells in each sample dish after removing the medium and washing the cells with phosphate-buffered saline (PBS). The weights of PEI max-coated MNPs in each 7.5 μ l sample of 1 mg/ml PEI max solution were 0.75, 1.5, 2.25, 3.0, 4.5, and 7.5 μ g for both γ -Fe₂O₃ and Fe₃O₄. The amount of plasmid DNA was 2.5 μ g for all the samples.

Each dish containing DNA/PEI max/MNP complexes was placed on a neodymium (NdFeB) permanent magnet (diameter = 40 mm, height = 20 mm) purchased from Sangyo Supply Co. for 1 h. Each dish containing DNA/PEI max/MNP complexes was excited using a magnetic field gradient perpendicular to the dish at 26.5–33.0 T/m in the area of the dish near the cell surface. Two days after transfection, its efficiency was evaluated by fluorescence microscopy. The areas of fluorescent cells in fluorescence micrographs were compared with those of all cells observed in phase-contrast micrographs. The ratio of area of the fluorescent cells was calculated. Nine datasets were prepared for each condition of the fluorescence micrographs (three dishes prepared for

each condition and three sites observed in each dish).

Cytotoxicity assay

HeLa cells were seeded in 35 mm dishes at a density of 200,000 cells/well. One day after the incubation, PEI max, PEI max-coated MNPs, DNA, DNA/PEI max complexes, and DNA/PEI max/MNP complexes were added to each dish. The method of transfection and preparation of each MNP density was the same as that for the transfection experiment. Two days after incubation, cell viability was evaluated by trypan blue dye exclusion test.

Size measurement

The hydrodynamic sizes of the PEI max-coated γ -Fe₂O₃ and Fe₃O₄ nanoparticles were measured by dynamic light scattering (DLS) method using a fiber-optical particle analyzer (FPAR-1000, Otsuka Electronics). The morphologies of the PEI max-coated γ -Fe₂O₃ nanoparticles and DNA/PEI max/ γ -Fe₂O₃ nanoparticle complexes were characterized by transmission electron microscopy (TEM).

Endocytic inhibitors

Chlorpromazine and genistein were used as endocytic inhibitors. Chlorpromazine (Nacalai Tesque) inhibits clathrin-dependent endocytosis (CDE), and genistein (Nacalai Tesque and Fujicco Co.) inhibits clathrin-independent endocytosis (CIE).

In the transfection experiment, HeLa cells (200,000 cells/well) were seeded in 35 mm dishes on the day prior to the initiation of the inhibition study. The cells were preincubated with endocytic inhibitors (10 μ g/ml chlorpromazine or 200 μ M genistein) in 1 ml/well of medium for 30 min. Endocytic inhibitors were also added during magnetofection and incubated for 1 h after magnetofection. Chlorpromazine was diluted in sterile water, and genistein was diluted in dimethyl sulfoxide (DMSO) so that the final concentration of DMSO in the medium was <0.1 % (Gruenstein et al. 1975; Rejman et al. 2005; Vercauteren et al. 2011).

Results and discussion

Dependency of transfection efficiency on weight of MNPs and cytotoxicity assay

Figure 1 illustrates the dependency of transfection efficiency on the weight of γ -Fe₂O₃ and Fe₃O₄ nanoparticles. Transfection efficiency increased with weight, but decreased with further increases in γ -Fe₂O₃ and Fe₃O₄ (>1.5 μ g). This dependency has been reported elsewhere (Plank et al. 2003; Kami et al. 2011a). For the weight of 1.5 and 2.25 μ g (γ -Fe₂O₃) and 1.5, 2.25, and 3.0 μ g (Fe₃O₄), differences in transfection efficiency were not significant ($p \geq 0.05$). The transfection efficiency of γ -Fe₂O₃ nanoparticles was higher compared with that of Fe₃O₄ nanoparticles at 0.75, 1.5, and 2.25 μ g ($p < 0.05$). Figure 2 is fluorescent micrographic images of γ -Fe₂O₃. These images also indicated the trend of transfection efficiency shown in Figs. 1 (2).

Figure 3 illustrates the viability of HeLa cells exposed to PEI max, PEI max-coated γ -Fe₂O₃ nanoparticles, DNA, DNA/PEI max complexes, and DNA/PEI max/ γ -Fe₂O₃ nanoparticle complexes. The weight of MNPs was 2.25 μ g (Fig. 3). The reduction in cell viability in cells exposed to PEI max and DNA compared with the control sample without PEI max, MNPs, or DNA was negligible ($p \geq 0.05$). The cell viability of the sample with PEI max-coated MNPs, DNA/PEI max complexes, and DNA/PEI max/MNP complexes decreased in contrast to the sample with only PEI max ($p < 0.05$). In addition, viability decreased significantly in the sample with DNA/PEI/max MNP complexes in comparison with the sample containing

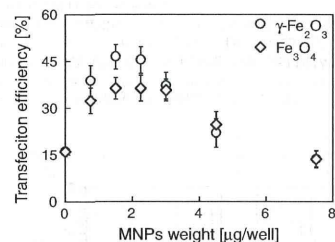


Fig. 1 Transfection efficiency as a function of magnetic nanoparticles (MNP) weight. Transfection efficiency was evaluated by fluorescent microscopy. MNP weight of 0 μ g/well indicates the sample containing DNA/polyethylenimine (PEI) max complexes

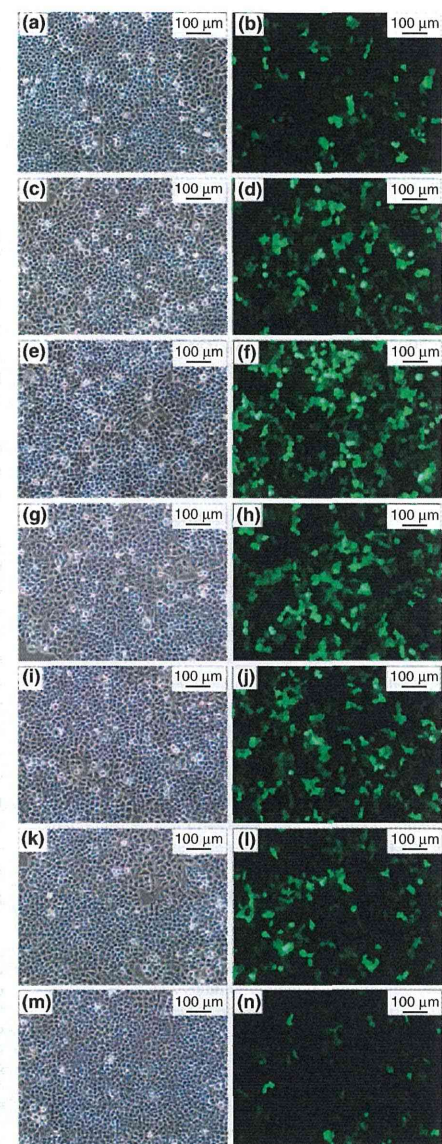
only DNA ($p < 0.05$). Figure 4 illustrates the dependency of cell viability on the weight of MNPs. Cell viability initially decreased with weight of MNPs; however, it increased with further increase in MNP weight (above 2.25 μ g; $p < 0.05$).

Decline in transfection efficiency has been attributed to cytotoxicity of DNA/MNPs (Plank et al. 2003). However, Figs. 1 and 4 show that cell viability in contrast to the decline in transfection efficiency, increased at higher MNP weights. In addition, the γ -Fe₂O₃ nanoparticle without coating has been reported to be of low cytotoxicity (Lee et al. 2011). It has been also reported that linear PEI has low cytotoxicity at lower concentrations, but is cytotoxic at higher concentrations (Banerjee et al. 2006; Jeong et al. 2001). In this study, the cytotoxicity of HeLa cells that were exposed to PEI max was significantly low because PEI max was used in low concentrations. Decline in cell viability in PEI max-coated γ -Fe₂O₃ nanoparticles is induced by reactive oxygen species due to the formation of free hydroxyl radical species, reacting with a range of intracellular constituents, due to high internalization of γ -Fe₂O₃ nanoparticles (McCord 1998; van der Bos et al. 2003; Arsianti et al. 2010b). However, this decline was minor because of the low doses of MNP incorporated into cells. Figures 3 and 4 suggest that the cytotoxicity may be attributed to high internalization of DNA/PEI max/MNP complexes into cells. The toxicity of DNA per se was negligible (Fig. 3). Internalization of DNA/PEI max/MNP complexes decreases cell viability, probably because of the disruption of cell membrane integrity after internalization (Prijic et al. 2012). The viability of HeLa cells exposed to complexes that contained γ -Fe₂O₃ nanoparticles of 2.25 μ g was reduced despite the low cytotoxicity of PEI max-coated γ -Fe₂O₃ nanoparticles. The sample with MNPs of 2.25 μ g induced higher transfection efficiency. This result suggests that cytotoxicity was because of higher internalization of DNA/PEI max/MNP complexes, and the trade-off between transfection efficiency and cytotoxicity is indicated (Arsianti et al. 2010b). The dependency of transfection efficiency and cell viability on the weight of MNPs indicates that transfection efficiency was not reduced because of cytotoxicity.

Aggregation of PEI max-coated MNPs

Figure 5 illustrates the size distribution of PEI max-coated γ -Fe₂O₃ and Fe₃O₄ nanoparticles in sterile

Fig. 2 Phase contrast (a, c, e, g, i, k, and m) and fluorescent (b, d, f, h, j, l, and n) micrographic images of transfected cells in the sample with γ -Fe₂O₃ of a, b 0, c, d 0.75, e, f 1.5, g, h 2.25, i, j 3.0, k, l 4.5, and m, n 7.5 μ g. MNP weight of 0 μ g/well indicates the sample containing DNA/polyethylenimine (PEI) max complexes



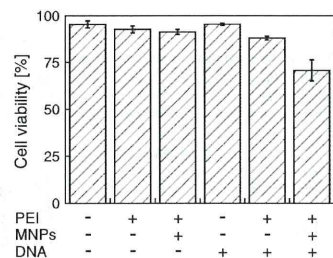


Fig. 3 Cell viability of HeLa cells in the presence of polyethylenimine (PEI) max, PEI max-coated γ -Fe₂O₃ nanoparticles, DNA, DNA/PEI max complexes, and DNA/PEI max/ γ -Fe₂O₃ nanoparticle complexes. The weight of magnetic nanoparticles (MNPs) was 2.25 μ g. The viability was evaluated by trypan blue dye exclusion test

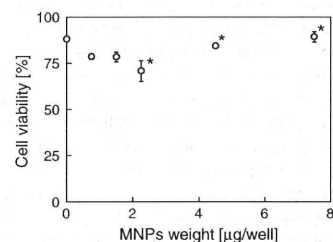
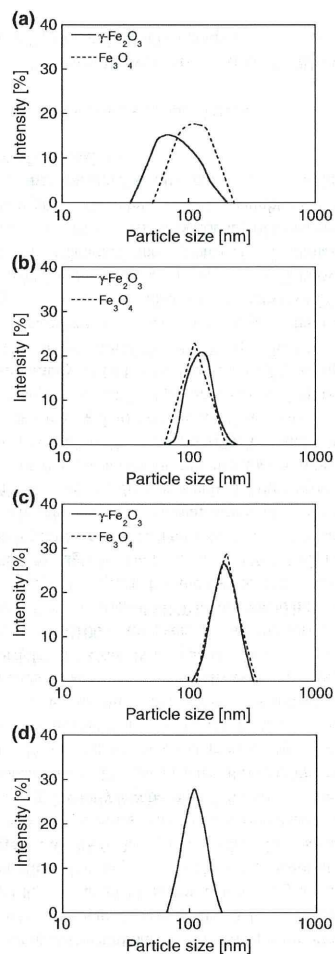


Fig. 4 Cell viability of HeLa cells as a function of the weight of polyethylenimine (PEI) max-coated γ -Fe₂O₃ nanoparticles. Magnetic nanoparticles (MNP) weight of 0 μ g/well indicates the sample containing DNA/PEI max complexes. Confirmation of the dependency of cell viability on the weight of MNPs is marked with asterisk ($p < 0.05$)

water (Fig. 5a), DNA/PEI max/ γ -Fe₂O₃ and Fe₃O₄ nanoparticle complexes in sterile water (Fig. 5b), the complexes in the medium (Fig. 5c) and pure medium, DMEM supplemented with 10 % FBS and 1 % PS (Fig. 5d) as measured by DLS. The diameters of PEI max-coated nanoparticles in sterile water were 84 \pm 31 nm (γ -Fe₂O₃) and 115 \pm 35 nm (Fe₃O₄). The diameters of DNA/PEI max/MNP complexes in sterile water were 126 \pm 27 nm (γ -Fe₂O₃) and 116 \pm 26 nm (Fe₃O₄). The diameters of the complexes in the medium were 191 \pm 39 nm (γ -Fe₂O₃) and 200 \pm 43 nm (Fe₃O₄). The size of the pure medium was 111 \pm 27 nm. These complexes included micro-size complexes, but this finding was not considered for evaluation in this study. In sterile



water, the size of PEI max-coated Fe₃O₄ nanoparticles is larger than that of PEI max-coated γ -Fe₂O₃ nanoparticles because the surface charge of bare Fe₃O₄ nanoparticles is lower than that of bare γ -Fe₂O₃ nanoparticles in the surface-coating process. In sterile water, bare Fe₃O₄ nanoparticles aggregate more readily than bare γ -Fe₂O₃ nanoparticles because the isoelectric point of Fe₃O₄ is nearer to the pH of sterile

Fig. 5 Size distribution of a polyethylenimine (PEI) max-coated γ -Fe₂O₃ and Fe₃O₄ nanoparticles in sterile water, b DNA/PEI max/ γ -Fe₂O₃ and Fe₃O₄ nanoparticle complexes in sterile water, c DNA/PEI max/ γ -Fe₂O₃ and Fe₃O₄ nanoparticle complexes in medium, and d pure medium (Dulbecco's modified Eagle medium supplemented with 10 % FBS and 1 % PS) as measured by dynamic light scattering (DLS). b and c were compared in the same condition as the ratio of DNA, PEI max, and magnetic nanoparticles (MNPs) to each other. The sizes were a 84 \pm 31 nm (γ -Fe₂O₃), 115 \pm 35 nm (Fe₃O₄), b 126 \pm 27 nm (γ -Fe₂O₃), 116 \pm 26 nm (Fe₃O₄), c 191 \pm 39 nm (γ -Fe₂O₃), 200 \pm 43 nm (Fe₃O₄), and d 111 \pm 27 nm. The complexes contained particles of micro-size, but this finding was not considered for evaluation in this study

water (pH 7.0) than that of γ -Fe₂O₃. Aggregation of PEI max-coated γ -Fe₂O₃ nanoparticles induced by DNA binding was confirmed (Fig. 5a, b). PEI max-coated Fe₃O₄ nanoparticles also aggregated because the complexes (both γ -Fe₂O₃ and Fe₃O₄) were of microsize (data not shown). PEI max-coated MNPs aggregate because of DNA binding. TEM observations also show that PEI max-coated MNPs aggregate because of conjugation with DNA (Fig. 6). Moreover, the medium induces additional aggregation of the complexes (Fig. 5b, c). The pH of culture medium is 7.4 (mildly alkaline), whereas that of sterile water is 7.0 (neutral). The positive surface charge of PEI-coated MNPs decreases owing to the mildly alkaline pH of the solvent. The complexes conjugate with serum protein contained in the medium. However, it has been reported that serum protein prevents the aggregation of MNPs modified with polymers (Wigo et al. 2012). The aggregation of the complexes in this study was reduced compared with serum-free medium because of serum proteins (data not shown).

A decrease in electrostatic repulsion due to DNA binding and mildly alkaline pH in the medium (pH 7.4) has been reported to induce aggregation of complexes (Arsianti et al. 2010a; Kami et al. 2011b; Miao et al. 2013). An increase in pH to a mildly alkaline level contributed to the instability of PEI-coated MNPs (Steitz et al. 2007; Wang et al. 2009). The models of aggregation for both γ -Fe₂O₃ and Fe₃O₄ nanoparticles are very similar.

Dependency of aggregation of DNA/PEI max/MNP complexes on weight of MNPs in the medium

Figures 7 and 8 illustrate the size distribution of the DNA/PEI max/ γ -Fe₂O₃ and Fe₃O₄ nanoparticle

complexes in the medium for weight of each of the MNPs as measured by DLS. The diameters of the γ -Fe₂O₃ complexes were 127 \pm 27, 124 \pm 24, 175 \pm 41, and 191 \pm 39 nm for samples with weights of 0.75, 2.25, 4.5, and 7.5 μ g, respectively. The diameters of the Fe₃O₄ complexes were 141 \pm 30, 144 \pm 30, 152 \pm 30, and 200 \pm 43 nm for the samples with the weight of 0.75, 2.25, 4.5, and 7.5 μ g, respectively. The samples contained micro-size complexes, but this finding was not considered for evaluation in this study. The size distributions indicated that aggregation was due to high weight of MNPs, except in the samples of 0.75 and 2.25 μ g as confirmed for γ -Fe₂O₃ and Fe₃O₄ complexes. This result indicates that the concentration of MNPs in the medium influences the aggregation of the complexes and that higher concentration induces higher aggregation. This aggregation affects transfection efficiency, which depends on the weight of MNPs (Fig. 1). The differences in transfection efficiency between γ -Fe₂O₃ and Fe₃O₄ are also influenced by the size of complexes. However, comparison of transfection efficiency between nanoparticles such as γ -Fe₂O₃ and Fe₃O₄ must take into account magnetization as a factor, influencing magnetic force on the particles (Johnson et al. 1975; Pankfurst et al. 2003; Furlani and Xue 2012).

In addition, the number of DNA/PEI max/MNP complexes was estimated by the following equation:

$$N = \frac{M}{VP} \quad (1)$$

where N is the number of complexes, M is the weight of MNPs used in each condition, V is the volume of complexes, and P is the bulk density of the MNPs. The volume was estimated by the following equation on the basis of the size distribution:

$$V = \sum_{k=1}^n \frac{4}{3} \pi \left(\frac{D_k}{2} \right)^3 F_k \quad (2)$$

where D is the diameter of the complexes, F is the fraction of the complexes of each diameter, and n is the number of measurement points. This estimate is rough because the complexes are not perfect spheres. However, this estimate gives excellent insight into the influence of MNP weight on transfection efficiency. The number of complexes decreased with increasing sizes of the complexes and the sizes

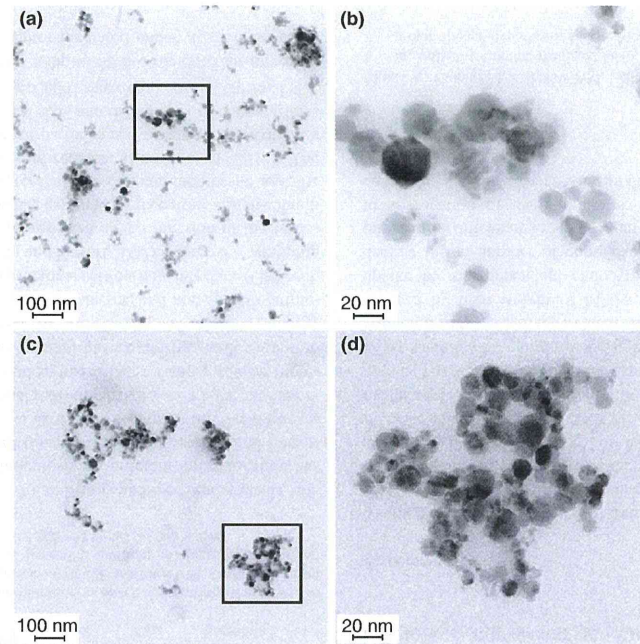


Fig. 6 Transmission electron microscopy (TEM) images of **a** polyethylenimine (PEI) max-coated magnetic nanoparticles (MNPs) (γ -Fe₂O₃ nanoparticles), **b** PEI max-coated MNPs magnified from **a**, **c** DNA/PEI max/MNP (2.25 μ g/well γ -Fe₂O₃

nanoparticle) complexes, **d** DNA/PEI max/MNP complex magnified from **c**. These were observed in sterile water. These images show that the complexes were larger than the PEI max-coated MNPs

increased because of aggregation. Figure 9 illustrates that the trend of transfection efficiency is according to the number of γ -Fe₂O₃ complexes. The number of complexes of size up to 200 nm was indicated by this estimate because higher internalization is confirmed to be achieved with nanoparticles of size up to 200 nm (Rejman et al. 2004). This trend was also confirmed for Fe₃O₄ complexes (data not shown). It is possible that aggregation affects transfection efficiency because of cellular uptake inhibition and reduction in the number of complexes.

Endocytic pathways of DNA/PEI max/MNP complexes

The endocytic pathways of the DNA/PEI/MNP complexes were similar to those of PEI polyplexes (Huth

et al. 2004). Endocytosis is divided into phagocytosis (the uptake of large particles) and pinocytosis (the uptake of fluids and solutes). Pinocytosis is classified into clathrin-dependent endocytosis (CDE) and clathrin-independent endocytosis (CIE) (Sahay et al. 2010). Nanoparticles with diameter up to 200 nm are internalized by CDE (Rejman et al. 2004), whereas nanoparticles that are not internalized by CDE enter the cells by CIE, for example caveolae- and flotillin-dependent endocytosis (Rejman et al. 2004; Payne et al. 2007). Flotillin-dependent endocytosis is PEI receptor (proteoglycan)-mediated pathway (Zanta et al. 1997; Zou et al. 2000), and proteoglycan is known as cell surface receptor binding cationic substrates (Mislick and Baldeschwieler 1996). Receptor-mediated endocytosis is induced by interaction between ligand and receptor bound to the cell surface.

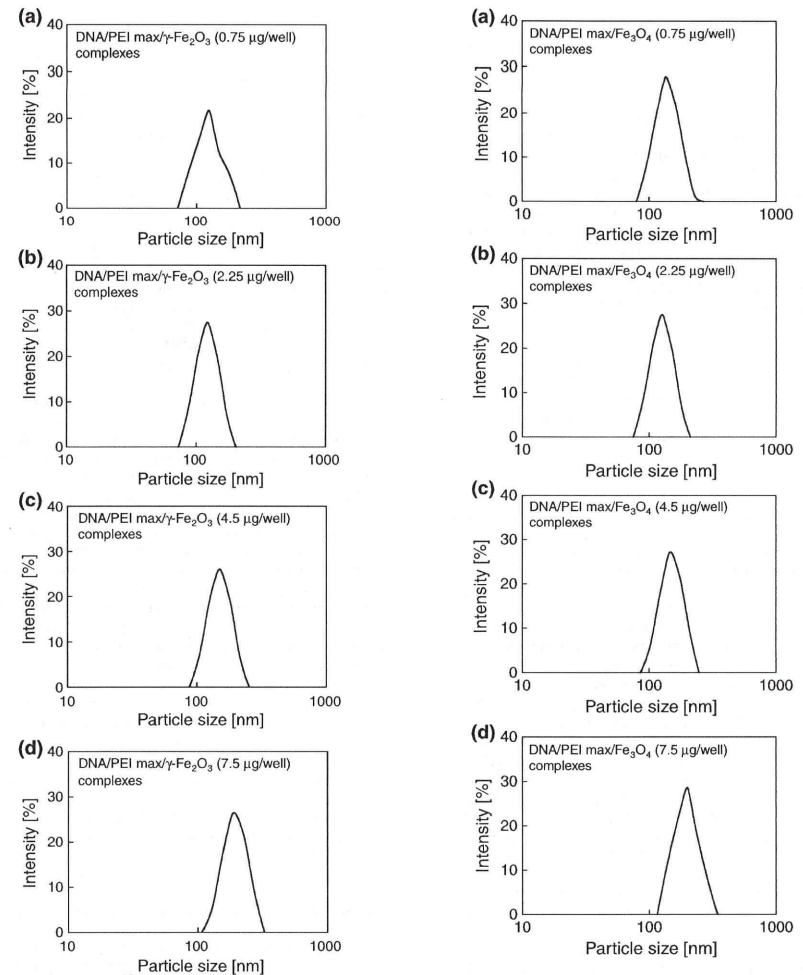


Fig. 7 Size distribution of DNA/polyethylenimine (PEI) max/ γ -Fe₂O₃ nanoparticle complexes in medium, as measured by dynamic light scattering (DLS) for **a** 0.75 μ g/well, **b** 2.25 μ g/well, **c** 4.5 μ g/well, and **d** 7.5 μ g/well, and the sizes of the complexes were **a** 127 ± 27 nm, **b** 124 ± 24 nm, **c** 152 ± 30 nm, **d** 191 ± 39 nm, respectively. The samples contained micro-order size complexes, but this finding was not considered for evaluation in this study

Fig. 8 The size distribution of DNA/polyethylenimine (PEI) max/Fe₃O₄ nanoparticle complexes in the medium as measured by dynamic light scattering (DLS) for **a** 0.75 μ g/well, **b** 2.25 μ g/well, **c** 4.5 μ g/well, **d** 7.5 μ g/well, and the size of the complexes were **a** 141 ± 30 nm, **b** 144 ± 30 nm, **c** 152 ± 30 nm, **d** 200 ± 43 nm, respectively. The samples contained micro-order size complexes, but this finding was not considered for evaluation in this study